Cellular and Molecular Life Sciences (2025) 82:308
https://doi.org/10.1007/s00018-025-05846-y

ORIGINAL ARTICLE

KRAS4B is required for placental development

Marie-Albane Minati[1] · Leyre López Muneta[1] · Younes Achouri[1] · Sophie Pirenne[1] · Corentin Porada[2] · Francesca Rochais[2] · Patrick Jacquemin[1]

Received: 8 April 2025 / Revised: 15 July 2025 / Accepted: 16 July 2025
© The Author(s) 2025

Abstract

Beyond its well-established role in cancer, KRAS is also crucial for embryogenesis, as its absence leads to embryonic lethality. However, the precise mechanisms underlying the developmental functions of KRAS, as well as the respective roles of its two splicing isoforms, KRAS4A and KRAS4B, remain incompletely characterized. To address these issues, we generated *Kras4A knock-out* (*Kras4A*$^{-/-}$) and *Kras4B*$^{-/-}$ mouse models using CRISPR/Cas9 technology, and compared their phenotypes to those of a *Kras*$^{-/-}$ model, in which both isoforms are simultaneously inactivated. We observed that *Kras*$^{-/-}$ and *Kras4B*$^{-/-}$ embryos show a lethality that starts around E13.5, while *Kras4A*$^{-/-}$ embryos develop normally, with no detectable abnormalities. In contrast, *Kras*$^{-/-}$ embryos displayed a dual phenotype affecting both the heart and placenta, whereas *Kras4B*$^{-/-}$ embryos exhibited only the placental phenotype. The cardiac phenotype was complex, combining ventricular non-compaction, ventricular septal defects, double outlet right ventricle, and overriding aorta, likely resulting from impaired cardiac precursor proliferation. The placental phenotype was characterized by reduced placental size, and a marked decrease in glycogen trophoblast cells, correlating with hypoglycemia and hypoxia in *Kras*$^{-/-}$ and *Kras4B*$^{-/-}$ embryos. Thus, our findings confirm the predominant role of KRAS4B in KRAS-mediated developmental functions, but also suggest hidden functions of KRAS4A. Importantly, this study is the first to identify KRAS as a key regulator of a specific cell differentiation process and to characterize the biological defects caused by its loss.

Keywords KRAS4A · KRAS4B · Development · Placenta · Heart

Introduction

The GTPase Kirsten rat sarcoma viral oncogene homolog (KRAS) has initially been identified by its oncological properties, and subsequently been shown to exhibit functions during mammalian embryogenesis. Studies about the developmental role of KRAS using knock-out (KO) mouse models have highlighted that the lack of KRAS induces severe growth defects resulting in *in utero* death around E15.5 [9, 11]. Detailed characterization of *Kras*$^{-/-}$ embryos revealed that they present features of anemia, fetal liver defect (decellularization) [9], motor neuronal defect (cell death), and ventricular myocardium atrophy [11].

The *Kras* gene is subject to an alternative splicing event which leads to the generation of two proteins, KRAS4A and KRAS4B. The two mRNA isoforms are differentiated by the presence of an alternative fourth exon. As this fourth exon is also the last one, this means that at the protein level, the two isoforms differ only by their C-terminal end. This C-terminus is essential for membrane targeting of both isoforms, a process that is essential for their activity. The two isoforms have a CAAX (cysteine - aliphatic amino acid - aliphatic amino acid - serine or methionine) consensus sequence at their end which is modified by the successive activity of three enzymes to lead to the addition of a farnesyl group at the C-terminal end [7]. Hydrophobicity created by this farnesylation is not sufficient to anchor KRAS4A and KRAS4B to the membrane. To increase the membrane affinity, KRAS4A undergoes a palmitoylation on a cysteine upstream to the CAAX motif while the KRAS4B uses a polybasic lysine domain. The fact that KRAS isoforms

✉ Patrick Jacquemin
patrick.jacquemin@uclouvain.be

[1] Université Catholique de Louvain, de Duve Institute, Brussels, Belgium

[2] Aix-Marseille Université, INSERM, Marseille Medical Genetics, Marseille, France

Published online: 13 August 2025

anchor to the membrane through different mechanisms suggests that both isoforms have distinct membrane localizations and/or functions.

An important question related to the functions of the two isoforms is their respective place and level of expression. In the absence of KRAS4A antibodies functioning in a reproducible manner, their expression pattern was determined at the transcription level by qRT-PCR. If *Kras4B* represents the major isoform in terms of expression level, *Kras4A* nevertheless shows dynamically and spatially regulated expression through embryogenesis [15]. A study of KRAS4A-deficient mice showed that these mice are healthy and fertile, indicating that KRAS4A is dispensable for embryonic development [16]. More recently, a study of KRAS4B-deficient mice found that these mice die perinatally [21]. They display heart abnormalities, strongly resembling those observed in $Kras^{-/-}$ embryos. These results indicate that the developmental functions of KRAS are most likely mediated by KRAS4B. Interestingly, however, it has been shown that KRAS4A can perform these functions as well, as mice with a *Kras4A* cDNA knockin in the *Kras* locus (preventing KRAS4B expression) are viable, with no apparent phenotype [5]. This suggests that the developmental properties of KRAS4B rely, at least in part, on its expression specificities.

Although informative about the roles of KRAS4A and KRAS4B during development, these different studies did not provide details on how KRAS (and its splicing isoforms) exerts its functions. To better understand the developmental functions of KRAS, we generated KRAS4A- or KRAS4B-deficient mouse models. We then characterized their phenotypes in detail, and performed a comparison with a mouse model of *Kras* inactivation (which loses both isoforms). Unexpectedly, we identified new roles for KRAS in heart septation and placenta development, the latter role being supported by KRAS4B.

Materials and methods

Mice

All procedures described in this study were performed with the approval of the animal welfare committee of the UCLouvain Health Sciences Sector (Brussels, Belgium, reference 2021/UCL/MD/054).

Embryos deficient in KRAS were generated by breeding $Kras^{LSL-G12D/+}$ mice [8] to obtain $Kras^{LSL-G12D/LSL-G12D}$ embryos. The presence of the LSL cassette precluding the transcription of the *Kras* gene, these mice cannot express KRAS and thus represent a model of functional Kras KO. For this reason, we call them here $Kras^{-/-}$.

Fig. 1 Generation of the $Kras4A^{-/-}$ and $Kras4B^{-/-}$ mouse models. (**A**) Scheme depicting the generation of the $Kras4A^{-/-}$ and $Kras4B^{-/-}$ models using CRISPR/Cas9. Genomic structure of the *Kras* locus is represented by white (non-coding sequences) and black boxes (coding-sequences). Exons 4A and 4B correspond to the green and blue boxes, respectively. The strategy used aims to insert or delete (indel) nucleotides in exons 4A and 4B by non-homologous DNA end-joining following Cas9 cleavage. (**B**) Nucleotide sequences of exons 4A and 4B, with the sequences corresponding to the single guide RNA used (yellow), and the PAM motifs (red). (**C**) Characteristics of the founders used to generate the $Kras4A^{-/-}$ and $Kras4B^{-/-}$ models. The codes (F…) correspond to the founder mice (2 founders per model). Indel indicates the number of nucleotides (N) inserted (Ins) and/or deleted (Del) in exons 4A or 4B for each model. Terminal amino acid sequence indicates the single-letter amino acid sequence encoded by exons 4A (green) and 4B (blue) from the *wild-type* allele, as well as the aa sequences predicted following the presence of indels in the different models. (**D**) Western blotting performed on liver extracts from embryos descending from the two founders (F605 and F606) of the $Kras4A^{-/-}$ colony and the two founders (F635 and F3575) of the $Kras4B^{-/-}$ colony. Due to the presumably lower expression of KRAS4A, no decreased KRAS expression (detected with an antibody recognizing both isoforms) is seen in $Kras4A^{-/-}$ embryos. KRAS4B expression (detected with an antibody specifically recognizing KRAS4B) is not affected in $Kras4^{-/-}$ mice. In $Kras4B^{-/-}$ embryos, KRAS4B expression is completely lost, while low KRAS4A expression is detected using the antibody recognizing both isoforms. Heat shock cognate protein 70 (HSC70) was used as loading control

$Kras4A^{-/-}$ and $Kras4B^{-/-}$ were generated using the cloning-free CRISPR-Cas9 system [1]. To target the mouse *Kras* gene we used CRISPRdirect software for designing the guide RNA (http://crispr.dbcls.jp/). The guide RNA was designed to target Kras exon 4A or 4B, as shown in Fig. 1. A ribonucleoprotein complex containing 2.4 pmol/µl crRNA/tracrRNA and 200 ng/µl Alt-R S.p. Cas9 Nuclease V3 (IDT, 1081059) was injected into the pronucleus of B6D2F2 mouse zygotes. Injected zygotes were transferred into oviduct of CD1 pseudo-pregnant female mice. Indel mutations were detected in the offspring by sequencing of PCR products. Breeding between $Kras4A^{\pm}$ mice generated $Kras4A^{-/-}$ mice, and breeding between $Kras4B^{\pm}$ mice generated $Kras4B^{-/-}$ mice.

$Kras^{Cit}$ mice expressing a Citrine-KRAS fusion protein (Cit-K) have been described [3]. All strains used in the present study were maintained in a CD1-enriched background.

Tetraploid complementation

Generation of tetraploid-diploid chimeras was performed as previously described [6]. Two-cell stage embryos were harvested from oviducts of E1.5 CD1 females and used to obtain tetraploid embryos by electrofusion. The blastomeres were electro-fused in culture medium containing 0.3 M mannitol. CF-150B pulse generator and an electrode with a 1000-µm gap were used. Two square 120 V pulses for 40 µs duration were applied. Embryos were washed and transferred into a drop of KSOM medium. Embryo fusion were

A

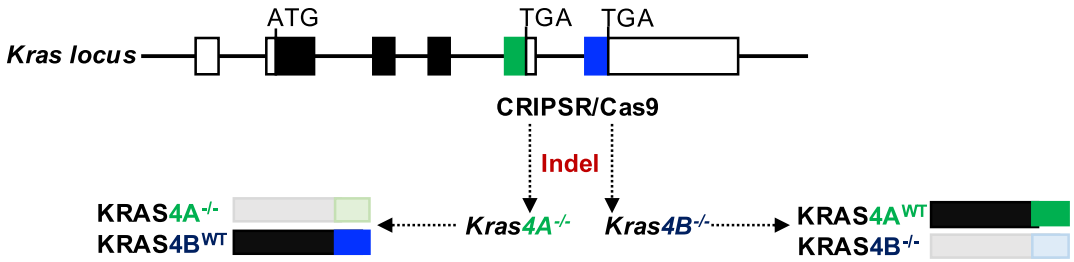

B

Exon 4A AGAGTGGAGGATGCTTTTTATACATTGGTGAGAGAGATCCGACAGTACAGATTGAAAAAA
ATCAGCAAAGAAGAAAAGACTCCTGGCTGTGTGAAAATTAAAAAATGCGTTATAATGTAA

Exon 4B GGTGTTGACGATGCCTTCTATACATTAGTCCGAGAAATTCGAAAACATAAAGAAAAGATG
AGCAAAGATGGGAAGAAGAAGAAGAAGAAGTCAAGGACAAGGTGTACAGTTATGTGA

C

	Founder	Indel	Terminal amino acid sequence
		Kras4A wild-type :	RVEDAFYTLVREIRQYRLKKISKEEKTPGCVKIKKCVIM (39 aa)
Kras4A-/-	F605	**Del-14N**	RVEDGERDPTVQIEKNQQRRKDSRLCEN (28 aa)
	F606	**Del-59N Ins-1N**	Undetermined (deletion in upstream intron and 5' part of 4A exon)
		Kras4B wild-type:	GVDDAFYTLVREIRKHKEKMSKDGKKKKKKSRTRCTVM (38 aa)
Kras4B-/-	F635	**Del-13N**	GVDDAFEKFENIKKR (15 aa)
	F3575	**Del-201N**	Undetermined (deletion in upstream intron and 5' part of 4B exon)

D

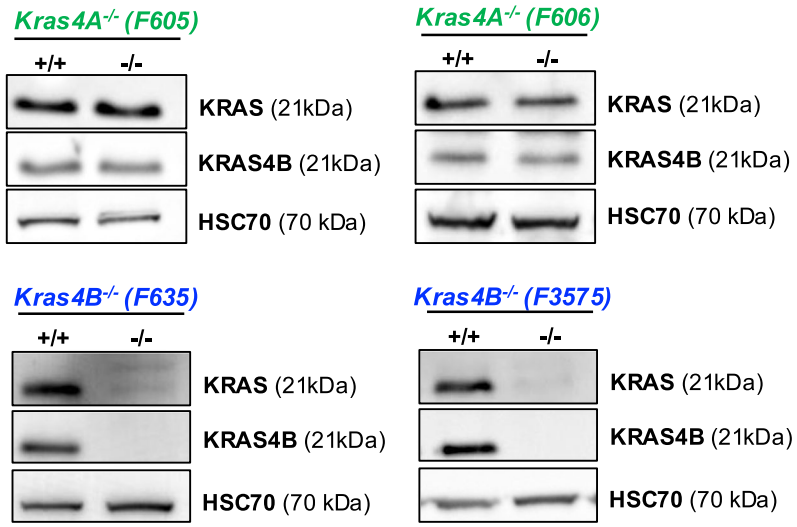

checked every 10–15 min under a stereo microscope. The fused embryos were transferred to a new drop of KSOM medium soon after fusion and allowed to develop to 4-cell stage (overnight at 37 °C, 5% C02). Eight-cell stage diploid embryos were harvested from oviducts of E2.5 *Kras*$^{\pm}$females mated with *Kras*$^{\pm}$ males. The zona pellucida of the embryos was dissolved in Acid Tyrode solution. The embryos were used immediately after to set up the aggregation. In each aggregation well, two tetraploid embryos "sandwiched" one diploid embryo. Embryos were then incubated at 37 °C, 5% CO2. The next day, the aggregates that have formed a single embryo were selected and transferred into the oviduct of CD1 mice. We transferred a total of 106 embryos; 18 E15.5 living embryos were recovered, of which only one was KO

for *Kras*, suggesting that *Kras*$^{-/-}$ embryos are particularly sensitive to in vitro manipulations.

Histological staining

Staining was performed on 6 µm-sections of formalin-fixed paraffin-embedded tissues. Tissue sections were deparaffinized 3 × 3 min in xylene, rehydrated in successive baths of 99%, 95%, 70%, 30% ethanol, and distillated water. For hematoxylin and eosin staining, sections were stained 14 s in Mayer's Hemalun solution (1.09249.1000, Millipore) and washed with tap water for 5 min. Then, sections were stained 7 s in Eosin solution (3137.2, Roth) and washed with tap water until stain fades. Periodic acid Shiff staining was performed using the Periodic Acid Shiff Staining Kit (395-1KT, Merck), following the manufacturer's protocol. After staining, tissue sections were shortly washed with 70%, 95% and 100% ethanol, and xylene before mounting slides with DPX (005790500, VWR).

Immunohistochemistry (IHC) and immunofluorescent labeling

Embryos were fixed for 6 h at 4 °C in 4% paraformaldehyde before embedding in paraffin. Six-mm tissue sections were deparaffinized and antigen retrieval was performed by heating the slides for 20 min in Tris–EDTA buffer (pH 9) in Lab Vision PT Module (Thermo Fisher Scientific) or for 10 min in citrate buffer (pH 6) in a microwave. Sections were washed 5 min in phosphate-buffered saline (PBS), and permeabilized in PBS, 0.3% Triton X-100 (Sigma Aldrich) for 5 min at room temperature (RT). Then, tissue sections were blocked in PBS, 3% low-fat milk, 10% bovine serum albumin (BSA), 0.3% Triton X-100 (blocking buffer) for 45 min at RT. Primary antibodies (Table 1) were diluted in blocking buffer and incubated with the samples overnight at 4 °C. Primary antibodies and antibody dilution are listed in Table 1. Then, slides were washed with PBS, 0.1% Triton X-100. Fluorescent-dye conjugated secondary antibodies were diluted in PBS, 10% BSA, 0.3% Triton X-100, applied at 1/1000 dilution, and incubated for 1 h at 37 °C. For IHC, secondary antibodies conjugated with the horseradish peroxidase were incubated with the samples at 37 °C for 1 h, before DAB staining.

For immunofluorescent labeling, pictures were taken with an Axiovert 200 fluorescent microscope (Zeiss) using the AxioVision software, or with Cell Observer Spinning Disk Confocal Microscope using the ZEN software. For IHC, pictures were selected after scanning performed on Pannoramic P250 Flash III (3DHistec). Quantifications were performed on at least 3–5 fields per stage/organ using the FIJI (ImageJ) or ZEN (Zeiss) softwares.

Table 1 Primary antibodies used

Antibodies	Origin	Experiment	Dilution	Reference
CD31	Rat	IF	1/250	Dianova (D130)
CD45	Rabbit	IHC	1/100	Abcam (ab10558)
Cleaved CASPASE3	Rabbit	IHC	1/200	Cell signaling (9661S)
GFP	Goat	IF	1/250	Abcam (ab6673)
HIF-1α	Rabbit	WB	1/500	Cell signaling (36169S)
ISL1	Mouse	IF	1/200	DHSB (39.4D5 and 40.2D6)
Ki67	Mouse	IHC	1/200	Abcam (ab16667)
KRAS	Rabbit	WB	1/250	Homemade
KRAS4B	Mouse	WB	1/250	Merck (WH0003845M1)
NCAM1	Rabbit	IF/IHC	1/200	Proteintech (14,255–1-AP)
PODXL	Mouse	IF	1/50	Bio-Techne (MAB1556)
STRA6	Rabbit	IF	1/100	Merck (ABN1662)
TER119	Rat	IHC	1/250	BD Bioscience (552,370)
TPBPA	Rabbit	IIHC	1/100	Abcam (ab104401)

Western blotting

Tissues at embryonic day (E)13.5 or E15.5 from *Kras*$^{-/-}$, *Kras4A*$^{-/-}$, *Kras4B*$^{-/-}$ or control *(+/+)* embryos were lysed in a buffer composed of 50 mM Tris–HCl (pH 7.4), 150 mM sodium chloride, 0.25% sodium deoxycholate, 1% NP-40, 1 mM sodium orthovanadate, 2% sodium dodecyl sulfate (SDS) and containing protease inhibitor cocktail (11836153001, Sigma Aldrich). Samples were kept on ice during the procedure. Then, samples were centrifuged (14000 g, 15 min, at 4 °C) to pellet cell debris. Proteins were quantified using a Bradford assay. Samples containing 30 or 50 mg total proteins were separated on 12.5% SDS polyacrylamide gels. PVDF membranes (ISEQ00010, Millipore) were blocked with a solution of 5% low-fat milk diluted in Tris-buffered saline (TBS), 0.1% Tween-20 (Sigma-Aldrich) for 1 h at RT. Membranes were incubated overnight at 4 °C with primary antibodies (listed in Table 1). Then, membranes were washed with TBS, 0.1% Tween-20 and incubated with secondary antibodies for 1 h at RT. After incubation, membranes were washed with TBS, 0.1% Tween-20 and revealed using SuperSignal™ West Pico PLUS Chemiluminescent Substrate (34577, Thermo Fisher), or SuperSignal™ West Femto Maximum Sensitivity Substrate (34095, Thermo Fisher). HSC70 was used as loading control. Pictures were taken with the Fusion Solo S imaging system (Viber). Densitometry was measured using the FIJI software (ImageJ), and the ratio of the protein of interest over HSC70 was calculated.

Detection of tissue hypoxia

Hypoxia was detected with both a HIF-1a antibody and the Hypoxyprobe kit (HP1, Hypoxyprobe). Hypoxyprobe kit consist of pimonidazole hydrochloride solution and mouse monoclonal antibody for detection of pimonidazole adducts in hypoxic tissue. Pimonidazole hydrochloride solution (60 mg/kg) was injected intravenously in E13.5 pregnant females. Two hours later, pregnant females were euthanized by cervical dislocation, and embryos with their placenta were collected. Then, samples were fixed in 4% paraformaldehyde for 6 h at 4 °C, before embedding in paraffin. Hypoxia, defined as partial pressure of oxygen (pO2) < 10 mmHg, was investigated on 6-mm transverse embryo and placenta sections using manufacturer's protocol, and visualized as brown stain following immunochemistry using DAB chromogen detection.

Blood glucose measurement

Embryonic blood were collected and glycemia were measured using a glucometer (Bayer Contour Next).

Statistical analysis

Data were presented as means ± standard error of the mean (SEM). Statistical significance of the difference between the percentage of KO embryos/mice that we have obtained compared to the expected 25% Mendelean percentage (Fig. 2A) was calculated by Chi-squared test. The percentages of KO embryos/mice per stages were calculated from total embryos/mice ranging from 38 to 200. For the other experiments, statistical significance of the difference between two groups (groups contain embryos/mice ranging from 3 to 10) was calculated using unpaired Student's t-test. For all statistical analyses, the level of significance was set at $p < 0.05$. Analyses were performed using GraphPad Prism software (version 9, GraphPad Software Inc). *, $p < 0.05$; **, $p < 0.01$; ***, $p < 0.001$; ****, $p < 0.0001$; ns, not significant.

Results

Generation of mouse models lacking the KRAS4A or KRAS4B isoform

To identify the specific roles of each isoform during embryonic development, we aimed to delete the C-terminus of each isoform which is required for targeting to the cell membrane and hence essential for their biological activity. To this end, we used the CRISPR/Cas9 technique to introduce an indel into the 5'part of exon 4 (Fig. 1A and B). Furthermore, this localization allows the elimination of the a5-helix which has been shown to be essential for the stability of KRAS4B, so that the protein generated following the presence of the indel is unstable and rapidly degraded [21]. For KRAS4A, AlphaFold predicts with very high confidence the presence of an α-helix at the corresponding sequence (https://alphafold.ebi.ac.uk/entry/P01116), suggesting that the loss of this sequence will also affect the stability of KRAS4A. The presence of this helix was recently confirmed by structural analysis of KRAS4A crystals [24]. This indicates that the loss of this sequence will also affect the stability of KRAS4A.

By following this strategy, two founders were identified for each model. One founder of the *Kras4A*$^{-/-}$ colony had a 14-nucleotide deletion and one founder of the *Kras4B*$^{-/-}$ colony had a 13-nucleotide deletion; proteins predicted from these deletions were 11 and 23 fewer amino acids than KRAS4A and KRAS4B, respectively (Fig. 1C). The other two founders had a deletion that moved up the intron upstream of exon 4, which did not allow us to predict the protein sequences encoded by these mutated alleles (Fig. 1C). In the 4 founders, the indels induced the loss of the stabilizing α-helix and the sequence allowing localization to the membrane.

In the absence of a reliable KRAS4A antibody, we sought to detect the presence of the mutant proteins by Western blot using antibodies for KRAS (detecting the two isoforms) and KRAS4B. For the two *Kras4A* founders, no difference was observed in the intensity of the 21 kDa bands obtained with the KRAS and KRAS4B antibodies for +/+ and -/- mice (Fig. 1D); this is very probably explained by the fact that the expression of the 4A isoform is markedly lower in the liver (organ used here as the source of the proteins tested in Western Blotting) than that of the 4B isoform [21]. Importantly, no band smaller than 21 kDa was observed with the KRAS antibody, indicating that the mutant forms were rapidly degraded, as expected. In addition, the loss of KRAS4A did not affect the expression level of KRAS4B, which was equivalent between the two genotypes (Fig. 1D. For both Kras4B founders, as expected, no band was observed with the KRAS4B antibody, while no band smaller than 21 kDa was found with the KRAS antibody; only two weak bands around 21 kDa, corresponding more probably to KRAS4A, were observed with the KRAS antibody (Fig. 1D). These results confirm that the generated mutations induce inactivations of the corresponding KRAS splicing isoforms.

Embryonic lethality observed in the absence of KRAS is associated with the loss of KRAS4B

To determine the respective role of each isoform in embryonic development, we were first interested in studying whether they are necessary for embryonic development.

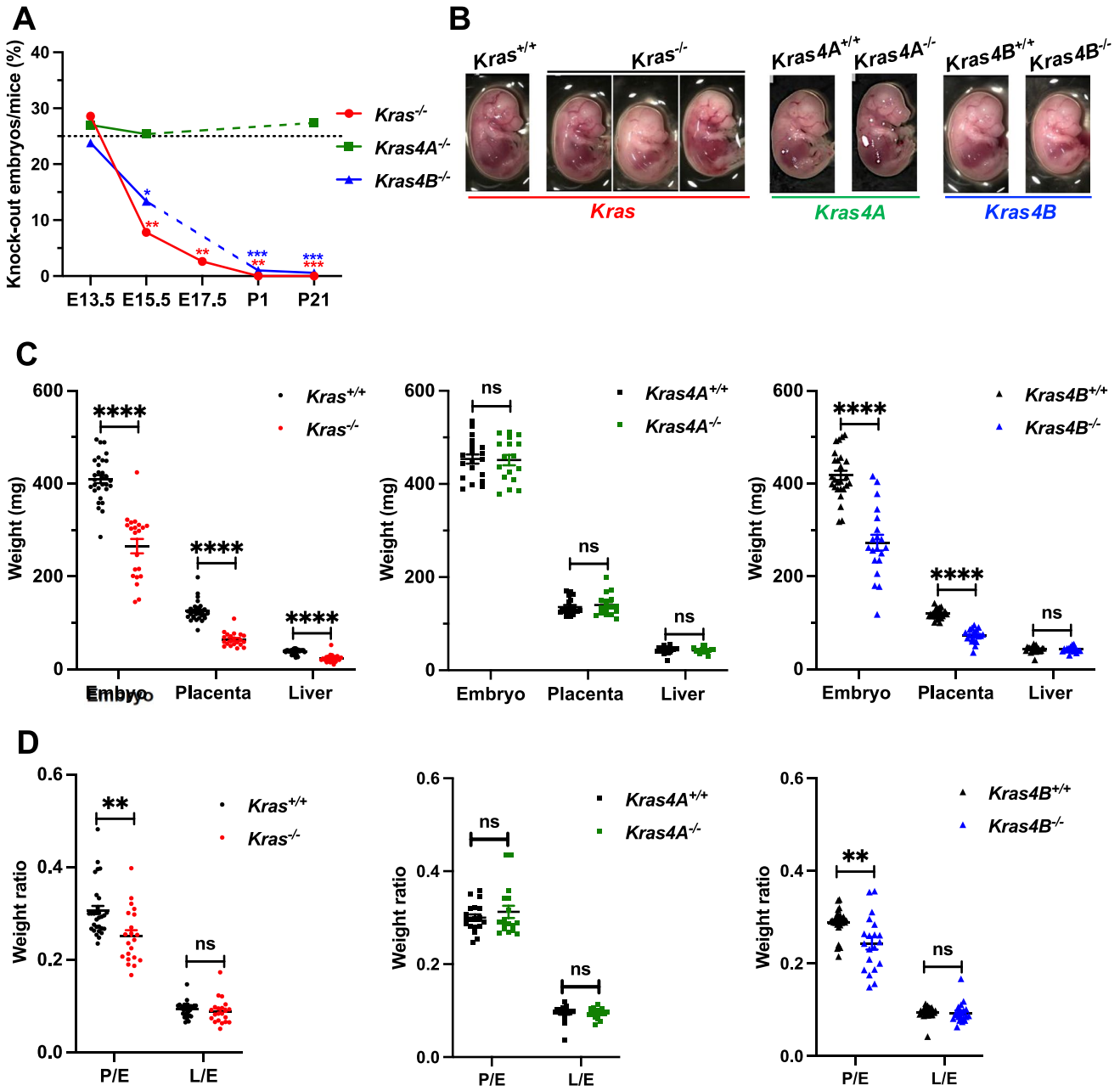

Fig. 2 *Kras*$^{-/-}$ and *Kras4B*$^{-/-}$ mice die in utero and have an impaired growth. (**A**) Percentage of *Kras*$^{-/-}$ (red line), *Kras4A*$^{-/-}$ (green line) and *Kras4B*$^{-/-}$ (blue line) mice as a function of the embryonic (E) or postnatal (P) stage. Black dot line represents the expected Mendelian percentage (25%) of knock-out (KO) embryos/mice. (**B**) Pictures showing the macroscopic phenotype of E15.5 embryos. *Kras*$^{-/-}$ embryos are frequently smaller and some of them present a paleness (embryo in the middle) and haemorrhagic signs (embryo on the right). *Kras4A*$^{-/-}$ embryos present a normal macroscopic phenotype whereas *Kras4B*$^{-/-}$ embryos are also frequently smaller. (**C**) Graphs showing the weight of E15.5 embryo, placenta and liver in the *Kras*$^{-/-}$, *Kras4A*$^{-/-}$ and *Kras4B*$^{-/-}$ models and their control (+/+) counterparts. (**D**) Graphs showing the placenta/embryo (P/E) and liver/embryo (L/E) weight ratios at E15.5 for the *Kras*$^{-/-}$, *Kras4A*$^{-/-}$ and *Kras4B*$^{-/-}$ embryos and their control (+/+) counterparts

For this, we analyzed the frequency of *Kras4A*$^{-/-}$ and *Kras4B*$^{-/-}$ embryos found at different embryonic stages and after birth, and compared these frequencies to those observed for *Kras*$^{-/-}$ embryos.

While *Kras4A*$^{-/-}$ mice are viable (Fig. 2A) and fertile (data not shown), embryonic lethality starting between E13.5 and E15.5 was observed both in *Kras*$^{-/-}$ and *Kras4B*$^{-/-}$ embryos (Fig. 2A). No statistically significant

difference was observed at E15.E between the survival percentage of Kras$^{-/-}$ and Kras4B$^{-/-}$ embryos. No *Kras*$^{-/-}$ mice were detected the day after birth, while rare *Kras4B*$^{-/-}$ (1/98 at P1 and 1/168 at P21) mice could be observed. Analysis of the macroscopic phenotype of E15.5 embryos highlighted that *Kras*$^{-/-}$ and *Kras4B*$^{-/-}$ embryos are characterized by a small size compared to control littermates; paleness and hemorrhages were also occasionally seen in *Kras*$^{-/-}$ embryos (Fig. 2B). The weight of KO embryos in both models was reduced by about 1.5 times compared to their littermates, as were their placenta weight (about 2.0 times lower) and the liver weight of *Kras*$^{-/-}$ embryos (Fig. 2C). When the organ/embryo weight ratio was calculated, no difference was nevertheless observed for the liver/embryo ratio between control and KO embryos, while for the placenta, a significantly lower ratio was observed for KO embryos (Fig. 2D). These results indicate that the mortality of *Kras*$^{-/-}$ embryos relies on the loss of KRAS4B. They suggest that KO placental function is defective, possibly explaining the smaller size of KO embryos.

The absence of KRAS does not impact cell proliferation or apoptosis

The smaller size of the KO embryos could be explained by a weaker proliferation. To evaluate this process, Ki67 immunostaining was performed on whole embryo sections. No difference was observed between control and *Kras*$^{-/-}$ embryos (Supllementary Fig. S1A). Similarly, we did not observe any difference in the level of apoptosis (Supplementary Fig. S1A). As these results are negative, we did not seek to confirm them for isoform knockouts, and therefore assume that KRAS4A and KRAS4B do not have roles in these processes by themselves. Our results contrast with those of previous studies that described increased apoptosis in neuronal tissues [11] and liver [9] of *Kras*$^{-/-}$ embryos. To ensure that apoptosis could not be decreased specifically in one of these organs, apoptosis was quantified more precisely in neuronal tissues and the liver; again, no difference was observed (Supplementary Fig. S1B).

However, we observed that some *Kras*$^{-/-}$ livers (about 40%) present an abnormal histology (Supplementary Fig. S2A), similar to the hypocellularity phenotype described in a previous study and possibly related to apoptotic process [9]. As our cleaved caspase-3 labeling does not support this hypothesis (see above), we explored other possible explanations. This could result from defective fetal liver hematopoiesis, however no difference was observed in the erythroid (TER199 immunostaining) and lymphoid (CD45 immunostaining) lineages between control and KO livers (Supplementary Fig. S2B). This could also originate from a dilation of the hepatic sinusoids. Importantly, a detailed pathological observation and CD31 immunolabeling led to the conclusion that it was indeed the case (inset in Supplementary Fig. S2A and C). In conclusion, as the liver phenotype remains mild, none of the experiments performed here can explain the reasons for the death of KO embryos, which must be sought elsewhere.

The absence of KRAS and, to a lesser extent, its splicing isoform KRAS4B impairs cardiac morphogenesis

Gross examination of tissue sections did not allow the identification of macroscopic phenotypes affecting the various organs of the *Kras*$^{-/-}$, *Kras4A*$^{-/-}$, and *Kras4B*$^{-/-}$ embryons, except for the *Kras*$^{-/-}$ and *Kras4B*$^{-/-}$ hearts for which the morphogenesis seems to be altered. To deepen this point, histological analysis of E15.5 hearts was performed and revealed conotruncal heart defects in 75% of the *Kras*$^{-/-}$ and 14% of the *Kras4B*$^{-/-}$ hearts, including ventricular septal defects (VSD; 6/8 and 1/7, respectively), double outlet right ventricle (DORV; 3/8 *Kras*$^{-/-}$), overriding aorta (oAo; 1/7 *Kras4B*$^{-/-}$) and ventricular non-compaction (NC; 5/8 *Kras*$^{-/-}$). No defect was observed in *Kras4A*$^{-/-}$ hearts or control littermates (0/6 and 0/31, respectively; $P<0.001$) (Fig. 3A and B).

Our results suggest that KRAS is required for arterial pole development and may control early cardiac progenitor cell deployment. To explore this possibility, we first performed immunofluorescence experiments on Citrine-KRAS E10.5 embryos [3] to explore the possibility that these cardiac progenitors express KRAS. This revealed preferential KRAS expression in Isl1^{+} cardiac progenitors (Fig. 3C). We then sought to verify whether the proliferation of these progenitors could be affected by the loss of KRAS, and found that it was reduced by approximately twofold in Kras$^{-/-}$ embryos (Fig. 3D). Together, these results support a role for KRAS in controlling cardiac progenitor cell development. Finally, to exclude any potential secondary impact of placental defects on cardiac morphogenesis, *Kras*$^{-/-}$ embryo tetraploid complementation was performed. Our results show that tetraploid complementation failed to rescue cardiac defects observed in *Kras*$^{-/-}$ mutant embryos (Fig. 3A and B; this suggests a direct role for KRAS in cardiac morphogenesis.

Placental cell differentiation and maternal blood sinuses are affected by the absence of KRAS and its splicing isoform KRAS4B

Since both KRAS and KRAS4B loss are associated with embryonic lethality, but *Kras4B*$^{-/-}$ embryos die without cardiac phenotype, it appears that the cardiac phenotype is not the cause of the death. To investigate the reason for this

A

	WT	*Kras*$^{-/-}$	*Kras4A*$^{-/-}$	*Kras4B*$^{-/-}$	Tetraploid compensated *Kras*$^{-/-}$
Total	31	8	6	7	1
Normal (%)	31 (100%)	2 (25%)	6 (100%)	6 (86%)	0
Defects (%)	0 0(%)	6 (75%)	0 (0%)	1 (14%)	1 (100%)
OAo	-	-	-	1	-
DORV	-	3	-	-	1
VSD	-	6	-	1	1
NC	-	5	-	-	1

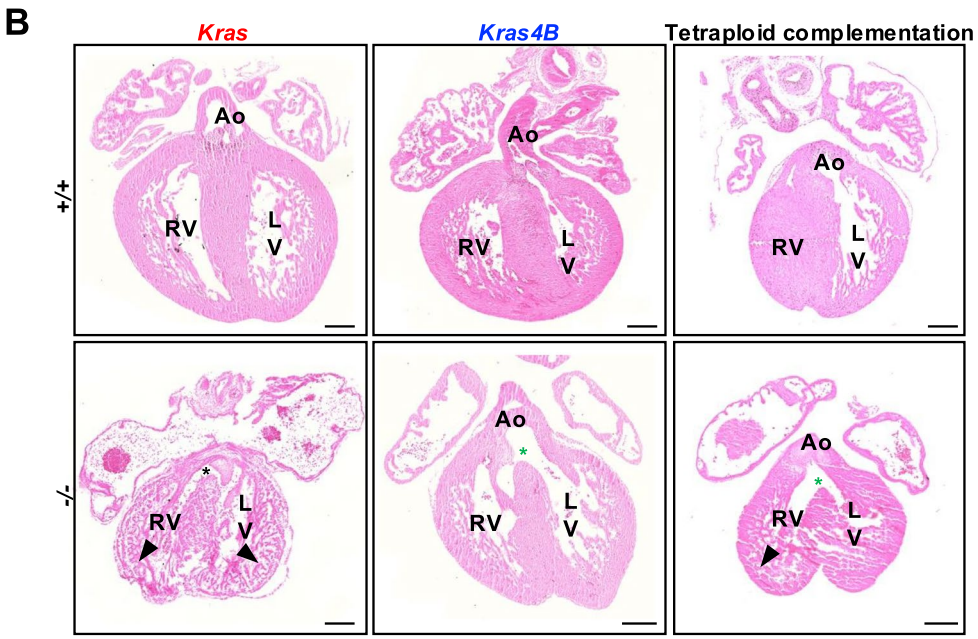

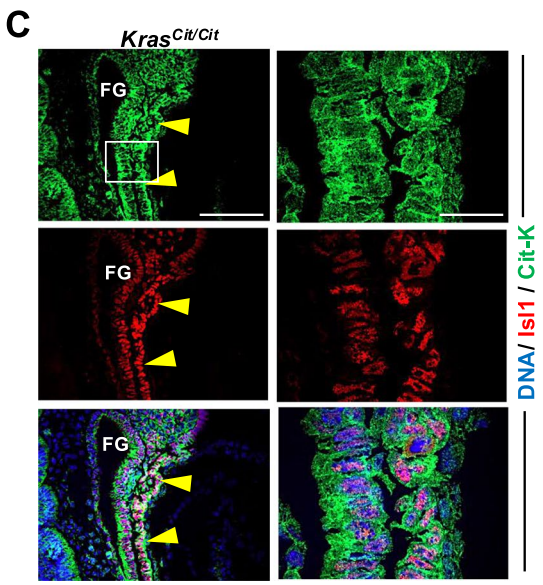

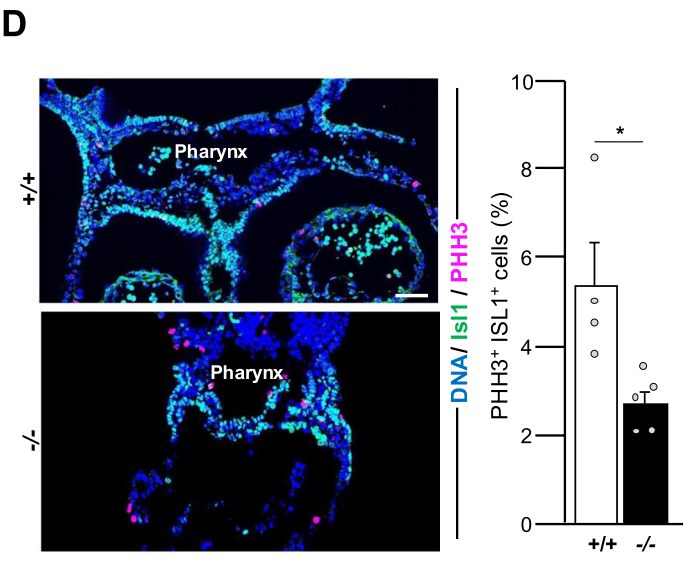

Fig. 3 *Kras*$^{-/-}$ and *Kras4B*$^{-/-}$ embryos, but not *Kras4A*$^{-/-}$ embryos, develop congenital heart defects. (**A**) Cardiac defects scored after analysis of histological sections at E15.5 *Kras*$^{-/-}$, *Kras4A*$^{-/-}$, *Kras4B*$^{-/-}$, tetraploid complemented *Kras*$^{-/-}$, and *Kras*$^{+/+}$ embryos. OAo, overriding aorta; DORV, double outlet right ventricle; VSD, ventricular septal defect; NC, non-compaction. (**B**) Eosin-stained sections of E15.5 hearts revealing that *Kras*$^{-/-}$, *Kras4B*$^{-/-}$, and tetraploid complemented *Kras*$^{-/-}$ embryos display congenital heart defects including membraneous ventricular septal defect (asterisk) associated with an overriding aorta (green asterisk) and ventricular non-compaction (arrowhead). Ao, aorta; LV, left ventricle; RV, right ventricle. Scale bars: 200 µm. (**C**) Immunofluorescent labelling for Citrine-Kras (Cit-K, using a GFP antibody) and Isl1 (for the cardiac progenitors) performed on E10.5 *Kras*$^{Cit/Cit}$ embryos. The white square corresponds to the magnified regions on the right. FG, foregut. Yellow arrow heads: cardiac progenitors. Scale bars: 100 µm, and 20 µm for the magnified regions. (**D**) Immunofluorescent labelling for Isl1 (for the cardiac progenitors) and PPH3 (for the proliferative cells) performed on control (+/+) and *Kras*$^{-/-}$ (-/-) E9.5 embryos. The position of the pharynx is indicated. Graphs showing the percentage of Isl1 + PHH3 + cells (cardiac progenitors) in the pharyngeal region of E9.5 *Kras*$^{-/-}$ (-/-) and control (+/+) embryons. Scale bar: 50 µm

lethality, we performed an analysis of KO placentas, as placental development appears to be defective in both models (see above).

While serial sections of placentas from the different models confirmed that the size of the *Kras*$^{-/-}$ and *Kras4B*$^{-/-}$ placentas were smaller, histological staining did not reveal any clearly visible disturbances in their general organization (Fig. 4A): staining with periodic acid-Schiff (PAS; stains glycogen trophoblast cells present in the junctional zone) and TPBPA (trophoblast-specific protein a; labels progenitors of many trophoblast subtypes found in the junctional zone), which allows to deliniate the two major layers of the mouse placenta, the junctional zone (JZ) and the labyrinth (L), showed that the relative surface of the two layers was not modified in the *Kras*$^{-/-}$ and *Kras4B*$^{-/-}$ placentas, in comparison to Kras$^{+/+}$ placentas (Supplementary Fig. S3). This indicates that the smaller size of KO placentas is not explained by a major perturbation in one of the two layers, but rather by a decrease in the absolute size of each of the layers.

Careful microscopic examination suggested that the maternal blood sinuses found in the labyrinth were enlarged in KO placentas. To clarify this point, we performed immunolabeling for PODXL, a marker for sinusoidal trophoblast giant cells (S-TGC) [12], which line the maternal blood sinuses. This labeling revealed approximately 2-fold enlargement of the maternal sinuses in *Kras*$^{-/-}$ and *Kras4B*$^{-/-}$ placentas, compared control placentas (Fig. 4B). PAS staining also suggested a decreased number of glycogen trophoblast cells (GC) in KO placentas. To explore this possibility, we performed NCAM1 immunostaining, and observed approximately 2 times less GC in *Kras*$^{-/-}$ and *Kras4B*$^{-/-}$ placentas than in control placentas (Fig. 4C). To verify that this phenotype is indeed cell-autonomous, we analyzed the expression of KRAS in the placenta using E15.5 *Kras*$^{Cit/Cit}$ embryos. A global view of the labyrinth layer showed extensive expression of KRAS (Supplementary Fig. S4A), while colabeling with NCAM revealed that KRAS was expressed in GC cells (Supplementary Fig. S4B; this indicates that the phenotype is likely cell-autonomous. Together, these results identify deficiencies in KO placentas and show for the first time that KRAS, through KRAS4B, is involved in the differentiation process of a specific cell type.

Hypoglycemia and hypoxia are detected in the absence of KRAS and its splicing isoform KRAS4B

The placental dysfunctions identified above could disrupt several of its functions, including glucose and oxygen supply to the embryo. To test this possibility, we first measured the glycemia of E15.5 embryos. While normal glycemia is observed in *Kras4A*$^{-/-}$ embryos, a 2-fold decrease in blood glucose was found in *Kras*$^{-/-}$ and *Kras4B*$^{-/-}$ embryos compared to control embryos (about 20 mg/dl vs 40 mg/dl) (Fig. 5A). This clearly shows that KO embryos suffer from hypoglycemia.

Oxygen levels were first estimated in E13.5 embryos and placentas using pimonidazole as a reductively activated probe in hypoxic cells (see Materials and methods for further explanation). In this way, we found a statistically significant nearly 3-fold increase in pimonidazole-protein adducts in *Kras*$^{-/-}$ embryos, and a statistically non-significant 1.5-fold increase in KO placentas, compared to control embryos and placentas (Fig. 5B). The presence of hypoxia in the *Kras*$^{-/-}$ and *Kras4B*$^{-/-}$ tissues was confirmed by detection of approximatively two-fold higher expression of HIF-1a in the latter (Fig. 5C). Taken together, these results show that vital biological parameters are already markedly disrupted in *Kras*$^{-/-}$ and *Kras4B*$^{-/-}$ embryos, moreover for hypoxia at a stage (E13.5) where mortality is not yet observed among these (see Fig. 2A).

Discussion

Although KRAS has been the subject of a tremendous amount of studies over the past 40 years, important aspects of its biology are still incompletely known. Thus, we know that KRAS is essential for embryonic development, but we do not yet know the mechanisms by which KRAS supports embryonic survival. Similarly, there are indications that its functions are carried out by its splicing isoform called KRAS4B, but a rigorous comparison of the respective roles of its two isoforms has never been performed. In the present work, we sought to answer these questions.

Our work shows similarities but also differences with previous studies [9, 11, 21]. Thus it confirms that embryos

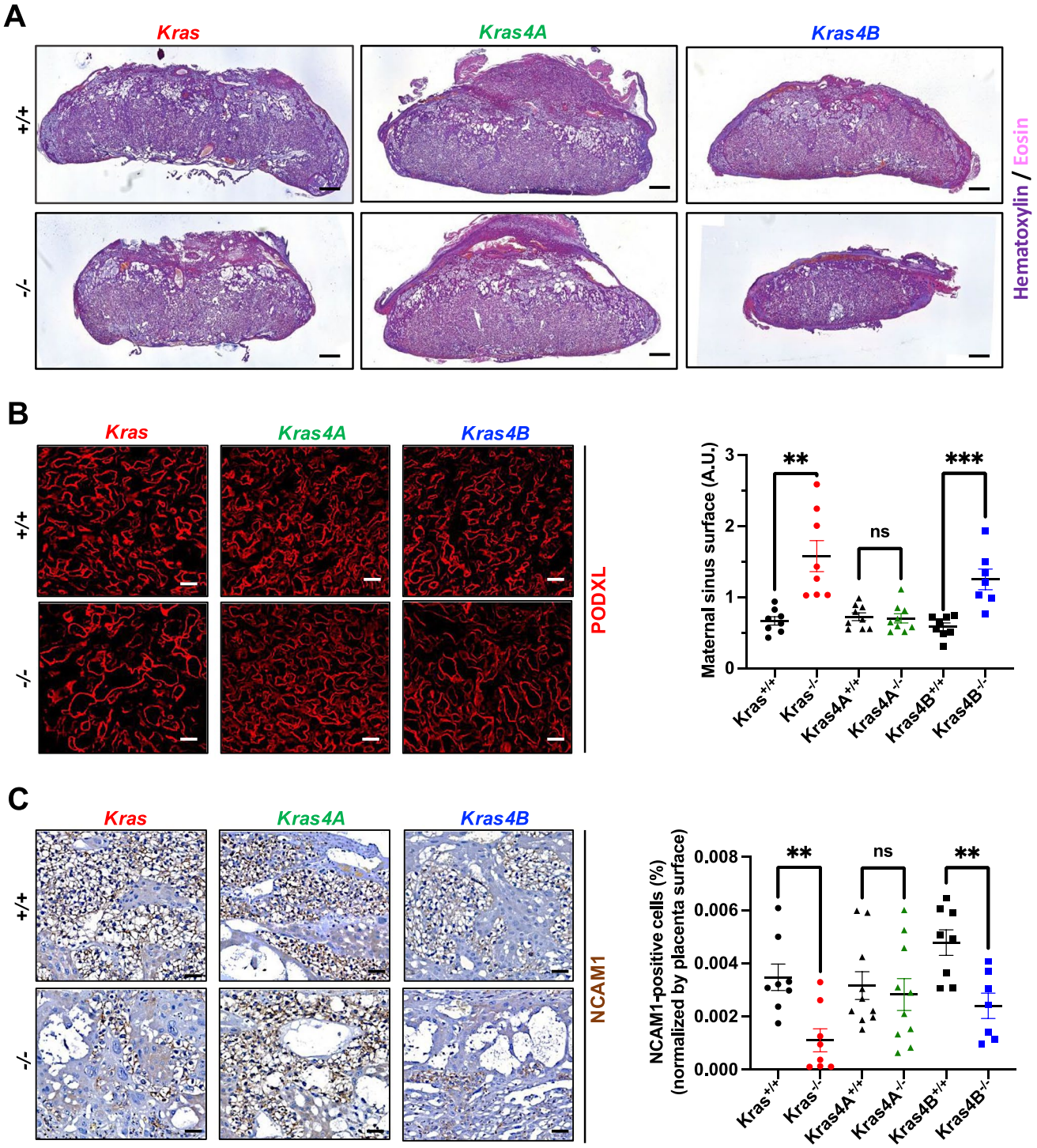

Fig. 4 Placental development is disrupted in *Kras*$^{-/-}$ and *Kras4B*$^{-/-}$ mouse models. (**A**) Hematoxylin and eosin staining performed on E15.5 placenta sections of *Kras, Kras4A*, and *Kras4B* control (+/+) and *knock-out* (-/-) embryos. Scale bar: 500 µm. (**B**) PODXL (Podocalyxin; marker of sinusoidal trophoblast giant cells surrounding the maternal blood sinuses) immunolabeling on E15.5 placenta from control (+/+), *Kras*$^{-/-}$, *Kras4A*$^{-/-}$ and *Kras4B*$^{-/-}$ embryos. Graph shows the surface of the maternal blood sinuses (A.U.: arbitrary unit) determined by FIDJI (Image J) software. One dot represents data obtained on a placenta. Scale bar: 50 µm. (**C**) NCAM1 (Neural Cell Adhesion Molecule 1; marker of glycogen trophoblast cells, in brown) immunostaining on E15.5 placenta from control (+/+), *Kras*$^{-/-}$, *Kras4A*$^{-/-}$ and *Kras4B*$^{-/-}$ embryos. Graph represents the quantification of the percentage of NCAM1-positive glycogen trophoblast cells normalized according to the surface of the placentas using Halo software. One dot represents data obtained on a placenta. Scale bar: 50 µm. Statistical significance between control (+/+) and *knock-out* (-/-) placentas of each model were tested by Student's t-test. Data are represented as mean±SEM. *, $p<0.05$; **; $p<0.01$; ***; $p<0.001$; ****; $p<0.0001$; ns, not significant

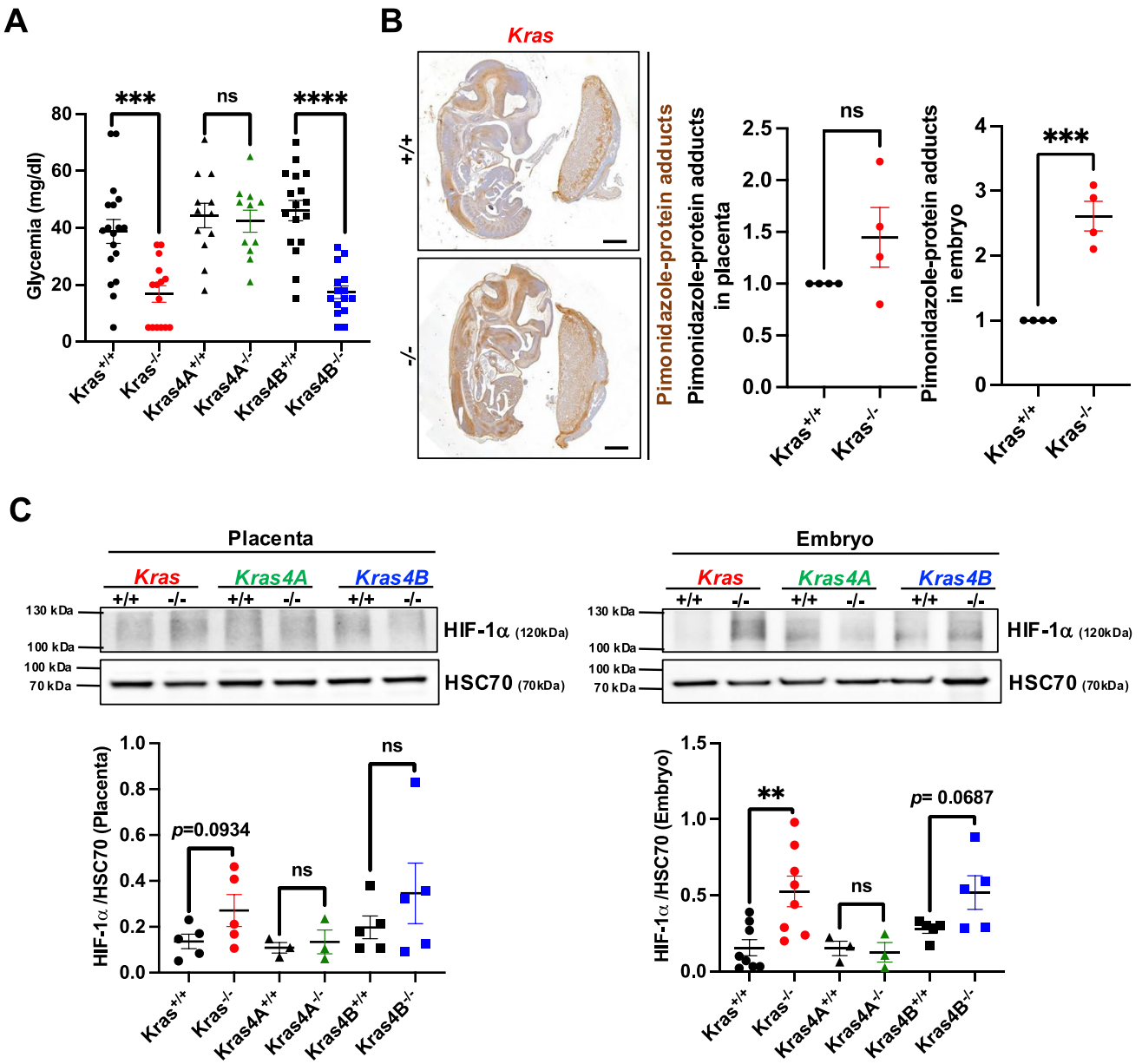

Fig. 5 Hypoglycemia and hypoxia are present in *Kras*$^{-/-}$ and *Kras4B*$^{-/-}$ embryos. (**A**) Glycemia of E15.5 *Kras*, *Kras4A*, and *Kras4B* control (+/+) and *knock-out* (-/-) embryos. Only KO embryos with still beating hearts were eligible for blood glucose measurements. (**B**) Detection of tissue hypoxia on transverse sections of E13.5 *Kras*$^{-/-}$ and control (+/+) placentas and embryos using pimonidazole hydrochloride (Hypoxyprobe) which generates piminidazole protein adducts (brown staining). Adduct levels were arbitrarily set to 1 in *Kras*$^{+/+}$ embryos. Scale bar: 1000 µm. (**C**) Western blot analysis on protein extracts from E13.5 *Kras*, *Kras4A*, and *Kras4B* control (+/+) and *knock-out* (-/-) placentas and embryos using an HIF-1α antibody to detect tissue hypoxia. Heat shock cognate protein 70 (HSC70) was used as loading control. Quantifications of the HIF-1α/HSC70 ratio were performed by FIJI software. On the graphs, one dot represents data obtained from one embryo. Statistical significance between control (+/+) and *knock-out* (-/-) samples were tested by Student's t-test. Data are represented as mean ± SEM. *, $p<0.05$; **, $p<0.01$; ***, $p<0.001$; ****, $p<0.0001$; ns, not significant

deficient in KRAS begin to die around E15.5, the differences between studies on the precise timing of mortality being easily attributable to differences in the genetic backgrounds of the mouse models used. The same explanation can be put forward for the presence of a previously described neuronal phenotype [11] that we do not observe, or for the cardiac phenotype which we describe and which is more complex than those already described [11, 21]. The major difference is the placental phenotype which we are the first to describe. As previous studies described relatively mild phenotypes which alone could not explain the observed early mortalities, we believe that this difference is not due to a question of background, but rather to the analysis of the placenta which was probably not performed in the previous studies.

Our study is also the first that within the same work generates mouse models with the inactivation of the different KRAS splicing isoforms and compares their phenotypes. We confirm that KRAS4B is the isoform that provides the majority of the developmental functions of KRAS, as both *Kras*$^{-/-}$ and *Kras4B*$^{-/-}$ models exhibit embryonic mortality and the same placental phenotype. However, our study suggests a minor role for KRAS4A that has not been identified so far. At first glance, KRAS4A has no function, as the *Kras4A*$^{-/-}$ model is not associated with lethality or any other phenotype. This minor role can be observed when comparing the survival curves of the *Kras*$^{-/-}$ and *Kras4B*$^{-/-}$ models. So we can see that *Kras4B*$^{-/-}$ embryos live a little longer than *Kras*$^{-/-}$ embryos. A similar observation was made in another study [21]. In addition, significantly fewer *Kras4B*$^{-/-}$ embryos develop a cardiac phenotype, compared to *Kras*$^{-/-}$ embryos. This shows that in these two situations, KRAS4A is able to compensate, at least partially, for the loss of KRAS4B. However, KRAS4A was unable to take over KRAS4B's role in the placenta. The reasons behind this partial compensation are not understood. This could be due to the fact that KRAS4A is not expressed in the placenta. Alternatively, KRAS4A could be expressed in the placenta but remain unpalmitoylated, thereby preventing its proper localization to the plasma membrane. Another possibility is that KRAS4A fails to interact with placenta-specific scaffold or adaptor proteins required for the assembly of functional signaling complexes essential for downstream KRAS signaling.

Interestingly, the simultaneous presence of cardiac and placental phenotypes is reminiscent of similar situations already observed in humans and mice [4, 10, 13, 20]. These situations contributed to the idea that there is a placenta-heart axis which refers to the existence of multiple common pathways that are critical for the development of the two organs [2]. Seeking to see if the placental phenotype was at the origin of the cardiac phenotype, we carried out a tetraploid complementation experiment. As we observe that the cardiac phenotype is still present after complementation, we conclude that the coexistence of these two phenotypes in *Kras*$^{-/-}$ embryos is not related to this axis, and that the cardiac phenotype is more likely explained by a role of KRAS in early heart development. To support this role, we show that KRAS is expressed in cardiac progenitors, in sharp contrast to its absence later in embryonic cardiomyocytes [14] and that the proliferation of these precursors is reduced in the absence of KRAS. Knowing that cardiac progenitor deployment is regulated by a complex network of signaling pathways and transcription factors controlling the balance between proliferation and differentiation [19] and that KRAS modulates multiple biological processes, including proliferation and differentiation, we cannot exclude any potential role for KRAS in controlling cardiac progenitor cell differentiation. However, compared to our previous studies [17], by themselves, the proliferation defects measured in KRAS mutant embryos may be largely sufficient to display the subsequently observed congenital heart defects.

The placental phenotype that we have identified in *Kras*$^{-/-}$ and *Kras4B*$^{-/-}$ embryos is dual. First, we observe a small placenta; strikingly, this reduction in size is even greater than that expected due to the reduced size of the KO embryos that we observe. This indicates that this reduction probably originates at an early stage of placental development. Hence, it supports a role of KRAS in amplifying a pool of trophoblast progenitors whose progeny will give rise to the different types of trophoblasts in the junctional and labyrinth zones. The second placental phenotype is a reduced number of GC. GC together with parietal trophoblast giant cells and spongiotrophoblast cells derive from tripotent precursors present in the ectoplacental cone; this suggests that KRAS also plays a more specific and late role in the commitment and/or proliferation of GC.

GC, located in the junctional zone and the decidua, have the ability to store glycogen, and as such, it has been assumed that they are an important source of glucose to support the growth of the embryo and placenta; accordingly, reduced placental glycogen content is frequently associated with embryonic growth restriction [23]. Thus, the decrease in GC could both explain the reduced size of KO placentas and embryos and the hypoglycemia found in the latter.

In addition to hypoglycemia, KO embryos also develop hypoxia, which suggests that maternal oxygen supply through the placenta is deficient. This supply takes place at an exchange interface located in the junctional zone. A thickening of this interface can lead to embryonic hypoxia [25], but our observations did not reveal such a thickening (data not shown). In contrast, the enlargement of the maternal blood sinuses found in KO placentas is accompanied by a statistically non-significant decrease of about 10% in the perimeter of the sinuses (data not shown), probably because these sinuses are less convoluted. This decrease, associated with the reduced size of the KO placentas, probably diminishes the exchange surface available with the maternal blood and consequently the maternal oxygen supply, and could thus partly explain the hypoxia of the KO embryos.

In humans, KRAS activating mutations are associated with the presence of rasopathies [18]. Conversely, no KRAS inactivating mutation has been associated to date with a human pathology. Based on the results obtained in mice, such a mutation could lead to cardiopathy or fetal lethality. Regarding the latter, exome sequencing of unexplained stillbirth did not identify a KRAS mutation in this condition [22]. For our part, we sequenced the different KRAS exons in a cohort of patients (n = 50) with heart disease and

for whom no mutations in known genes involved in these pathologies had been identified. Interestingly, we found the presence of a single nucleotide deletion in the 3'UTR of KRAS appearing in the heterozygous state in 17 patients (data not shown). As this mutation has never been identified before in 224,316 sequenced KRAS alleles, it will be interesting to study the consequences of its presence on the level of KRAS expression.

In conclusion, our study has reinforced the knowledge of KRAS functions during embryonic development, revealing a role of KRAS in the placenta and showing that KRAS was able to control the differentiation process of a type of trophoblast.

Supplementary Information The online version contains supplementary material available at https://doi.org/10.1007/s00018-025-05846-y.

Acknowledgements We thank Dr Fanny Bajolle for providing patient samples from CARREG study (France; CNIL; No. 1734573V0, supported by Association pour la Recherche en Cardiologie du Fœtus à l'Adulte (ARCFA)). The authors also thank the members of the LPAD laboratory for help and discussions, Maxime Libert for COSD acquisition, Jean-Nicolas Lodewycks and Hajar Dahou for mouse genotyping, and Bruno Maricq for his help with mouse care.

Author contributions MM and PJ contributed to conception and design of the study. MM and FR performed the data acquisition. MM performed the statistical analysis. YA generated the mouse models and performed the tetraploid complementation. SP performed the histopathological analysis of the liver. MM, SP, FR and PJ performed the data analysis. MM and PJ performed the data interpretation. MM and PJ wrote the manuscript.

Funding This work was supported by grants from the Université catholique de Louvain (Fonds Spéciaux de Recherche) and the FRS-FNRS (#J.0085.19) to PJ. MM and SP hold a Televie fellowship. PJ is Research Director at FRS-FNRS, Belgium.

Data availability The data that support the results of this study are available from the corresponding author.

Declarations

Conflict of interest The authors declare that the research was conducted in the absence of any commercial or financial relationships that could be construed as a potential conflict of interest.

Open Access This article is licensed under a Creative Commons Attribution-NonCommercial-NoDerivatives 4.0 International License, which permits any non-commercial use, sharing, distribution and reproduction in any medium or format, as long as you give appropriate credit to the original author(s) and the source, provide a link to the Creative Commons licence, and indicate if you modified the licensed material. You do not have permission under this licence to share adapted material derived from this article or parts of it. The images or other third party material in this article are included in the article's Creative Commons licence, unless indicated otherwise in a credit line to the material. If material is not included in the article's Creative Commons licence and your intended use is not permitted by statutory regulation or exceeds the permitted use, you will need to obtain permission directly from the copyright holder. To view a copy of this licence, visit http://creativecommons.org/licenses/by-nc-nd/4.0/.

References

1. Aida T, Chiyo K, Usami T, Ishikubo H, Imahashi R, Wada Y, Tanaka KF, Sakuma T, Yamamoto T, Tanaka K (2015) Cloning-free CRISPR/Cas system facilitates functional cassette knock-in in mice. Genome Biol 160:87
2. Andescavage NN, Limperopoulos C (2021) Placental abnormalities in congenital heart disease. Transl Pediatr 10:214–2156
3. Assi M, Achouri Y, Loriot A, Dauguet N, Dahou H, Baldan J, Libert M, Fain JS, Guerra C, Bouwens L, Barbacid M, Lemaigre FP, Jacquemin P (2021) Dynamic regulation of expression of KRAS and its effectors determines the ability to initiate tumorigenesis in pancreatic acinar cells. Cancer Res 81:2679–2689
4. Barak Y, Sadovsky Y, Shalom-Barak T (2008) PPAR signaling in placental development and function. PPAR Res 2008:142082
5. Chen WC, To MD, Westcott PMK, Delrosario R, Kim IJ, Philips M, Tran Q, Bollam SR, Goodarzi H, Bayani N, Mirzoeva O, Balmain A (2021) Targeting KRAS4A splicing through the RBM39/DCAF15 pathway inhibits cancer stem cells. Nat Comm 12:4288
6. Eakin GS, Hadjantonakis AK (2006) Production of chimeras by aggregation of embryonic stem cells with diploid or tetraploid mouse embryos. Nat Protoc 1:1145–1153
7. Haidar M, Jacquemin P (2021) Past and future strategies to inhibit membrane localization of the kras oncogene. Int J Mol Sci 22:13193
8. Jackson EL, Willis N, Mercer K, Bronson RT, Crowley D, Montoya R, Jacks T, Tuveson DA (2001) Analysis of lung tumor initiation and progression using conditional expression of oncogenic K-ras. Genes Dev 15:3243–3248
9. Johnson L, Greenbaum D, Cichowski K, Mercer K, Murphy E, Schmitt E, Bronson RT, Umanoff H, Edelmann W, Kucherlapati R, Jacks T (1997) K- ras is an essential gene in the mouse with partial functional overlap with N- ras. Genes Dev 11:2468–2481
10. Jones HN, Olbrych SK, Smith KL, Cnota JF, Habli M, Ramos-Gonzales O, Owens KJ, Hinton AC, Polzin WJ, Muglia LJ, Hinton RB (2015) Hypoplastic left heart syndrome is associated with structural and vascular placental abnormalities and leptin dysregulation. Placenta 36:1078–1086
11. Koera K, Nakamura K, Nakao K, Miyoshi J, Toyoshima K, Hatta T, Otani H, Aiba A, Katsuki M (1997) K-Ras is essential for the development of the mouse embryo. Oncogene 15:1151–1159
12. Marsh B, Blelloch R (2020) Single nuclei RNA-seq of mouse placental labyrinth development. Elife 9:e60266
13. Matthiesen NB, Henriksen TB, Agergaard P, Gaynor JW, Bach CC, Hjortdal VE, Østergaard JR (2016) Congenital heart defects and indices of placental and fetal growth in a nationwide study of 924 422 liveborn infants. Circulation 134:1546–1556
14. Minati MA, Assi M, Libert M, Cordi S, Lemaigre F, Jacquemin P (2022) *KRAS* protein expression becomes progressively restricted during embryogenesis and in adulthood. Front Cell Dev Biol 10:995013
15. Newlaczyl AU, Coulson JM, Prior IA (2017) Quantification of spatiotemporal patterns of Ras isoform expression during development. Sci Rep 7:41297
16. Plowman SJ, Williamson DJ, O'Sullivan MJ, Doig J, Ritchie AM, Harrison DJ, Melton DW, Arends MJ, Hooper ML, Patek CE (2003) While K-ras is essential for mouse development, expression of the K-ras 4A splice variant is dispensable. Mol Cell Biol 23:9245–9250

17. Rammah M, Théveniau-Ruissy M, Sturny R, Rochais F, Kelly RG (2022) PPARγ and NOTCH regulate regional identity in the murine cardiac outflow tract. Circ Res 131:842–858
18. Rauen KA (2013) The RASopathies. Annu Rev Genomics Hum Genet 14:355–369
19. Rochais F, Mesbah K, Kelly RG (2009) Signaling pathways controlling second heart field development. Circ Res 104:933–942
20. Rychik J, Goff D, McKay E, Mott A, Tian Z, Licht DJ, Gaynor JW (2018) Characterization of the placenta in the newborn with congenital heart disease: distinctions based on type of cardiac malformation. Pediatr Cardiol 39:1165–1171
21. Salmón M, Paniagua G, Lechuga CG, Fernández-García F, Zarzuela E, Álvarez-Díaz R, Musteanu M, Guerra C, Caleiras E, Muñoz J, Ortega S, Drosten M, Barbacid M (2021) KRAS4A induces metastatic lung adenocarcinomas in vivo in the absence of the KRAS4B isoform. Proc Natl Acad Sci U S A 118:e2023112118
22. Stanley KE, Giordano J, Thorsten V, Buchovecky C, Thomas A, Ganapathi M, Liao J, Dharmadhikari AV, Revah-Politi A, Ernst M, Lippa N, Holmes H, Povysil G, Hostyk J, Parker CB, Goldenberg R, Saade GR, Dudley DJ, Pinar H, Hogue C, Reddy UM, Silver RM, Aggarwal V, Allen AS, Wapner RJ, Goldstein DB (2020) Causal genetic variants in stillbirth. N Engl J Med 383:1107–1116
23. Tunster SJ, Watson ED, Fowden AL, Burton GJ (2020) Placental glycogen stores and fetal growth: insights from genetic mouse models. Reproduction 159:R213–R235
24. Whitley MJ, Tran TH, Rigby M, Yi M, Dharmaiah S, Waybright TJ, Ramakrishnan N, Perkins S, Taylor T, Messing S, Esposito D, Nissley DV, McCormick F, Stephen AG, Turbyville T, Cornilescu G, Simanshu DK (2024) Comparative analysis of KRAS4a and KRAS4b splice variants reveals distinctive structural and functional properties. Sci Adv 10:eadj4137
25. Winterhager E, Zenclussen AC, Plösch T, Perez-Garcia V, Hemberger M, Woods L (2018) Regulation of placental development and its impact on fetal growth-new insights from mouse models. Front Endocrinol 9:570

Publisher's Note Springer Nature remains neutral with regard to jurisdictional claims in published maps and institutional affiliations.